Global Journal of Researches in Engineering: F
Electrical and Electronics Engineering
Volume 23 Issue 3 Version 1.0 Year 2023
Type: Double Blind Peer Reviewed International Research Journal
Publisher: Global Journals
Online ISSN: 2249-4596 & Print ISSN: 0975-5861

Joint Sequential use of the Reassigned Smoothed Pseudo Wigner-Ville Distribution and the Hough Transform vs. the Reassigned Smoothed Pseudo Wigner-Ville Distribution for Detecting and Characterizing Low Probability of Intercept Triangular Modulated Frequency Modulated Continuous Wave Radar Signals in Low Signal to Noise Ratio Environments

By Daniel L. Stevens

Abstract- Digital intercept receivers are moving away from Fourier-based analysis towards classical time-frequency analysis techniques along with other novel analysis techniques for the purpose of analyzing low probability of intercept radar signals. This paper presents a novel approach of the joint sequential use of the Reassigned Smooth Pseudo Wigner-Ville Distribution and the Hough Transform versus the Reassigned Smooth Pseudo Wigner-Ville Distribution for characterizing low probability of intercept triangular modulated frequency modulated continuous wave radar signals. The metrics used for evaluation were - percent error of the chirp rate, percent detection, and lowest signal-to-noise ratio for signal detection. Experimental results demonstrate that overall, the joint sequential use of the Reassigned Smooth Pseudo Wigner-Ville Distribution and the Hough Transform signal processing techniques produced more accurate metrics than the Reassigned Smooth Pseudo Wigner-Ville Distribution signal processing technique. An improvement in the accuracy of metrics may well equate to an increase in personnel safety.

GJRE-F Classification: *FOR Code: 0906*

Joint Sequential use of the Reassigned Smoothed Pseudo Wigner-Ville Distribution and the Hough Transform vs. the Reassigned Smoothed Pseudo Wigner-Ville Distribution for Detecting and Characterizing Low Probability of Intercept Triangular Modulated Frequency Modulated Continuous Wave Radar Signals in Low Signal to Noise Ratio Environments

Daniel L. Stevens

Abstract- Digital intercept receivers are moving away from Fourier-based analysis towards classical time-frequency analysis techniques along with other novel analysis techniques for the purpose of analyzing low probability of intercept radar signals. This paper presents a novel approach of the joint sequential use of the Reassigned Smooth Pseudo Wigner-Ville Distribution and the Hough Transform versus the Reassigned Smooth Pseudo Wigner-Ville Distribution for characterizing low probability of intercept triangular modulated frequency modulated continuous wave radar signals. The metrics used for evaluation were - percent error of the chirp rate, percent detection, and lowest signal-to-noise ratio for signal detection. Experimental results demonstrate that overall, the joint sequential use of the Reassigned Smooth Pseudo Wigner-Ville Distribution and the Hough Transform signal processing techniques produced more accurate metrics than the Reassigned Smooth Pseudo Wigner-Ville Distribution signal processing technique. An improvement in the accuracy of metrics may well equate to an increase in personnel safety.

I. Introduction

The Low Probability of Intercept (LPI) signal used for this paper is the Frequency Modulated Continuous Wave (FMCW) signal, which is commonly used in modern radar systems [WAN10], [WON09], [WAJ08]. The frequency modulation spreads the transmitted energy over a large modulation bandwidth ΔF, providing good range resolution that is essential for discriminating targets from clutter. The power spectrum of the FMCW signal is nearly rectangular over the modulation bandwidth, so non-cooperative interception can be a challenge. Since the transmit waveform is deterministic, the form of the return signals can be predicted. This gives it the added advantage of being resistant to interference (such as jamming), since any signal not matching this form can be suppressed [WIL06]. Consequently, it is difficult for an intercept receiver to detect the FMCW waveform and measure the parameters accurately enough to match the jammer waveform to the radar waveform [PAC09].

Author: Air Force Research Laboratory, Rome, NY.
e-mail: daniel.stevens.7@us.af.mil

The most prevalent linear modulation utilized is the triangular FMCW emitter [LIA09], since it can measure the target's range and Doppler [MIL02], [LIW08]. Triangular modulated FMCW is the waveform that is employed for this paper.

Time-frequency signal analysis involves the analysis and processing of signals with time-varying frequency content. These signals are best represented by a time-frequency distribution [PAP95], [HAN00], which shows how the energy of the signal is distributed over the two-dimensional time-frequency plane [WEI03], [LIX08], [OZD03]. Processing of the signal can exploit the features produced by the concentration of signal energy in two dimensions (time and frequency), instead of in one dimension (time or frequency) [BOA03], [LIY03]. Noise tends to spread out evenly over the time-frequency domain, whereas signals concentrate their energies within limited time intervals and frequency bands; therefore, the local SNR of a 'noisy' signal can be improved simply by using time-frequency analysis [XIA99]. In addition, the intercept receiver can increase its processing gain simply by implementing time-frequency signal analysis [GUL08].

Time-frequency representations are valuable for the visual interpretation of signal dynamics [RAN01]. An experienced operator can more easily detect a signal and extract the signal parameters by analyzing a time-frequency representation, vice a time representation, or a frequency representation [ANJ09].

One of the members of the time-frequency analysis techniques family is the Wigner-Ville Distribution (WVD). The WVD has several desirable mathematical properties: it is always real-valued, it preserves time and frequency shifts, and it satisfies marginal properties [QIA02]. The WVD is computed by correlating the signal with a time and frequency translated version of itself, making it bilinear. The WVD has the highest signal energy concentration in the time-frequency plane [WIL06]. By using the WVD, an intercept receiver can come close to having a processing gain near the LPI radar's matched filter processing gain [PAC09]. The WVD, however, contains cross term interference

Global Journal of Research in Engineering (F) XXIII Issue III Version I Year 2023

between each pair of signal components, which may limit its applications [GUL07], [STE96], and which can make the WVD time-frequency representation hard to read, especially if the components are numerous or close to each other, and the more so in the presence of noise [BOA03]. This lack of readability may equate to less accurate signal detection and parameter extraction metrics, potentially placing the intercept receiver signal analyst's platform in harm's way.

The WVD of a signal $x(t)$ is given in equation (1) as:

$$W_x(t,f) = \int_{-\infty}^{+\infty} x(t+\frac{\tau}{2})x^*\left(t-\frac{\tau}{2}\right)e^{-j2\pi f\tau}\,d\tau \tag{1}$$

or equivalently in equation (2) as:

$$W_x(t,f) = \int_{-\infty}^{+\infty} X(f+\frac{\xi}{2})X^*\left(f-\frac{\xi}{2}\right)e^{j2\pi \xi t}\,d\xi \tag{2}$$

A lack of readability must be overcome to obtain time-frequency distributions that can be easily read by operators and easily included in a signal processing application [BOA03].

Some efforts have been made recently in that direction, and in particular, a general methodology referred to as reassignment.

The original idea of reassignment was introduced to improve the Spectrogram [OZD03]. As with any other bilinear energy distribution, the Spectrogram is faced with an unavoidable trade-off between the reduction of misleading interference terms and a sharp localization of the signal components.

We can define the Spectrogram as a two-dimensional convolution of the WVD of the signal by the WVD of the analysis window, as in equation (3):

$$S_x(t,f;h) = \iint_{-\infty}^{+\infty} W_x(s,\xi)W_h(t-s,f-\xi)dsd\xi \tag{3}$$

Therefore, the distribution reduces the interference terms of the signal's WVD, but at the expense of time and frequency localization. However, a closer look at equation (3) shows that $W_h(t-s,f-\xi)$ delimits a time-frequency domain at the vicinity of the (t,f) point, inside which a weighted average of the signal's WVD values is performed. The key point of the reassignment principle is that these values have no reason to be symmetrically distributed around (t,f), which is the geometrical center of this domain. Therefore, their average should not be assigned at this point, but rather at the center of gravity of this domain, which is much more representative of the local energy distribution of the signal [AUG94]. Reasoning with a mechanical analogy, the local energy distribution $W_h(t-s,f-\xi)W_x(s,\xi)$ (as a function of s and ξ) can be considered as a mass distribution, and it is much more accurate to assign the total mass (i.e. the Spectrogram value) to the center of gravity of the domain rather than to its geometrical center. Another way to look at it is this: the total mass of an object is assigned to its geometrical center, an arbitrary point which except in the very specific case of a homogeneous distribution, has no reason to suit the actual distribution. A much more meaningful choice is to assign the total mass of an object, as well as the Spectrogram value, to the center of gravity of their respective distribution [BOA03].

This is precisely how the reassignment method proceeds: it moves each value of the Spectrogram computed at any point (t,f) to another point $(\hat{t},\hat{f})$ which is the center of gravity of the signal energy distribution around (t,f) (see equations (4) and (5)) [LIX08]:

$$\hat{t}(x;t,f) = \frac{\iint_{-\infty}^{+\infty} sW_h(t-s,f-\xi)W_x(s,\xi)dsd\xi}{\iint_{-\infty}^{+\infty} W_h(t-s,f-\xi)W_x(s,\xi)dsd\xi} \tag{4}$$

$$\hat{f}(x;t,f) = \frac{\iint_{-\infty}^{+\infty} \xi W_h(t-s,f-\xi)W_x(s,\xi)dsd\xi}{\iint_{-\infty}^{+\infty} W_h(t-s,f-\xi)W_x(s,\xi)dsd\xi} \tag{5}$$

and thus, leads to a reassigned Spectrogram (equation (6)), whose value at any point (t',f') is the sum of all the Spectrogram values reassigned to this point:

$$S_x^{(r)}(t',f';h) = \iint_{-\infty}^{+\infty} S_x(t,f;h)\delta\left(t'-\hat{t}(x;t,f)\right)\delta\left(f'-\hat{f}(x;t,f)\right)dtdf \tag{6}$$

One of the most interesting properties of this new distribution is that it also uses the phase information of the STFT, and not only its squared modulus as in the Spectrogram. It uses this information from the phase spectrum to sharpen the amplitude estimates in time and frequency. This can be seen from the following expressions of the reassignment operators:

$$\hat{t}(x;t,f) = -\frac{d\Phi_x(t,f;h)}{df} \tag{7}$$

$$\hat{f}(x;t,f) = f + \frac{d\Phi_x(t,f;h)}{dt} \tag{8}$$

where $\Phi_x(t,f;h)$ is the phase of the STFT of x: $\Phi_x(t,f;h) = \arg(F_x$ (t, f; h)). However, these expressions (equations (7) and (8)) do not lead to an efficient implementation, and must be replaced by equations (9) (local group delay) and (10) (local instantaneous frequency):

$$\hat{t}(x;t,f) = t - \Re\left\{\frac{F_x(t,f;T_h)F_x^*(t,f;h)}{\left|F_{x(t,f;h)}\right|^2}\right\} \tag{9}$$

$$\hat{f}(x;t,f) = f - \Im\left\{\frac{F_x(t,f;D_h)F_x^*(t,f;h)}{\left|F_{x(t,f;h)}\right|^2}\right\} \tag{10}$$

where $T_h(t) = t \times h(t)$ and $D_h(t) = \frac{dh}{dt}(t)$. This leads to an efficient implementation for the Reassigned Spectrogram without explicitly computing the partial derivatives of phase. The Reassigned Spectrogram may thus be computed by using 3 STFTs, each having a different window (the window function h; the same window with a weighted time ramp t*h; the derivative of the window function h with respect to time (dh/dt)). Reassigned Spectrograms are therefore very computationally efficient to implement.

Since time-frequency reassignment is not a bilinear operation, it does not permit a stable reconstruction of the signal. In addition, once the phase information has been used to reassign the amplitude coefficients, it is no longer available for use in reconstruction. For this reason, the reassignment method has received limited attention from engineers, and its greatest potential seems to be where reconstruction is not necessary, that is, where signal analysis is an end unto itself.

One of the most important properties of the reassignment method is that the application of the reassignment process to any distribution of Cohen's class theoretically yields perfectly localized distributions for chirp signals, frequency tones, and impulses. This is one of the reasons that the reassignment method was chosen for this paper as a signal processing technique for analyzing LPI radar waveforms such as the triangular modulated FMCW waveforms (which can be viewed as back-to-back chirps).

To rectify the classical time-frequency analysis deficiency of cross-term interference, a method needs to be utilized that reduces cross-terms, which the reassignment method does.

The reassignment principle for the Spectrogram allows for a straight-forward extension of its use for other distributions as well [HIP00], including the WVD. If we consider the general expression of a distribution of the Cohen's class as a two-dimensional convolution of the WVD, as in equation (11):

$$C_x(t,f;\Pi) = \iint_{-\infty}^{+\infty} \Pi(t-s,f-\xi)W_x(s,\xi)dsd\xi \tag{11}$$

replacing the particular smoothing kernel $W_h(u,\xi)$ by an arbitrary kernel $\Pi(s,\xi)$ simply defines the reassignment of any member of Cohen's class (equations (12) through (14)):

$$\hat{t}(x;t,f) = \frac{\iint_{-\infty}^{+\infty} s\Pi(t-s,f-\xi)W_x(s,\xi)dsd\xi}{\iint_{-\infty}^{+\infty} \Pi(t-s,f-\xi)W_x(s,\xi)dsd\xi} \tag{12}$$

$$\hat{f}(x;t,f) = \frac{\iint_{-\infty}^{+\infty} \xi\Pi(t-s,f-\xi)W_x(s,\xi)dsd\xi}{\iint_{-\infty}^{+\infty} \Pi(t-s,f-\xi)W_x(s,\xi)dsd\xi} \tag{13}$$

$$C_x^{(r)}(t',f';\Pi) = \iint_{-\infty}^{+\infty} C_x(t,f;\Pi)\delta\left(t'-\hat{t}(x;t,f)\right)\delta\left(f'-\hat{f}(x;t,f)\right)dtdf \tag{14}$$

The resulting reassigned distributions (which includes the Reassigned Smooth Pseudo Wigner-Ville Distribution (RSPWVD)) efficiently produce a reduction of the interference terms provided by a well-adapted smoothing kernel. In addition, the reassignment operators $\hat{t}(x;t,f)$ and $\hat{f}(x;t,f)$ are very computationally efficient [AUG95].

P.V.C. Hough patented the Hough transform in 1962 [HOU62], and it was later used in work accomplished by Duda and Hart [DUD72].

Consider the case where we have straight lines in an image. For every point (x_i, y_i) in the image, all the straight lines pass through that point satisfy $y_i = mx_i + c$ for varying values of line slope and intercept.

Now if we reverse our variables and look instead at the values of (m, c) as a function of the image point coordinates (x_i, y_i), then $y_i = mx_i + c$ becomes $c = y_i - mx_i$ which also describes a straight line.

Consider two points $p1$ and $p2$, which lie on the same line in the (x, y) space. For each point, we can represent all possible lines through it by a single line in the (m, c) space. Therefore, a line in the (x, y) space that passes through both points must lie on the intersection of the two lines in the (m, c) space representing the two points. This means that all points which lie on the same line in the (x, y) space are represented by lines which all pass through a single point in the (m, c) space.

To avoid the problem of infinite m values which occurs when vertical lines exist in the image, an alternative formulation, $\rho = x\cos\theta + y\sin\theta$ (the parametric representation of a line) can be used to describe a line [CAR94], [DAH08]. This means that a point in the (x, y) space (image space) is now represented by a sinusoid in (ρ, θ) space (parameter space) rather than by a straight line. Points lying on the same line in the (x, y) space define sinusoids in the parameter space which all intersect at the same point. The more points that exist on that particular line in image space; the more sinusoids will intercept at that particular point in parameter space, and consequently, the more the accumulator value at this point (parameter space) will increase, forming a 'spike' in the parameter space. Therefore, 'spikes' (peak values) in the parameter space correspond to lines in the image space. The coordinates of the point of intersection of the sinusoids in the parameter space define the parameters of the line in the (x, y) space (image space). For example, if we apply the Hough transform to the WVD of a chirp (line), we obtain a peak in the parameter space located in a position which depends on the parameter values (such as chirp rate) of the chirp (line) in the image space (the WVD plot) [SHA07] [XUL93].

This can best be shown by Figure 1 below:

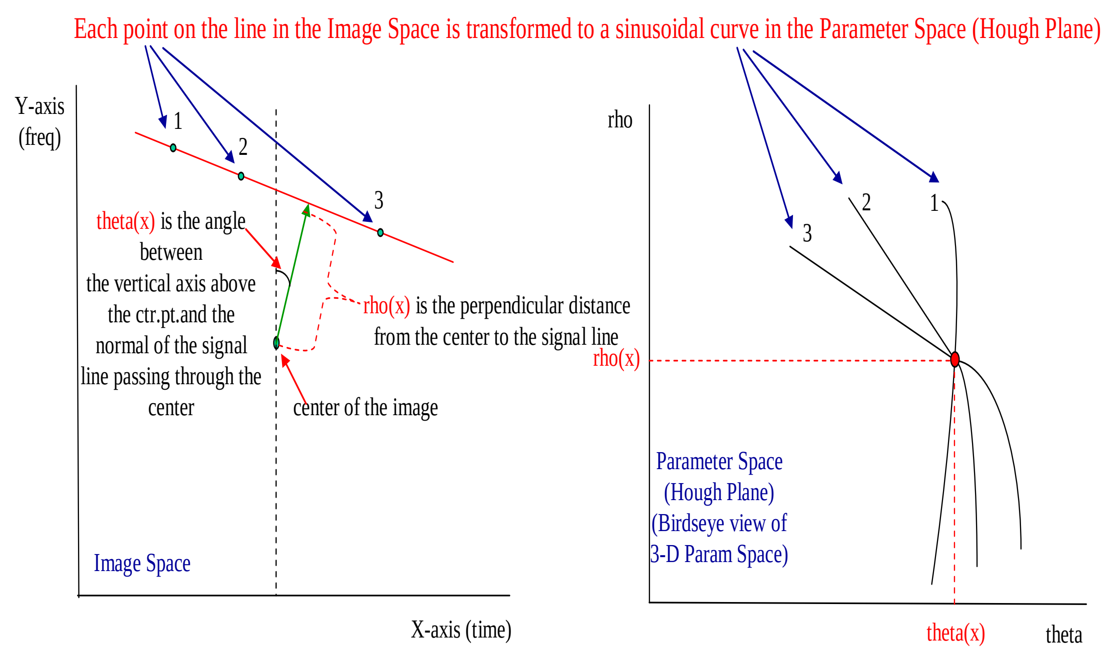

Figure 1: Time-frequency plot on the left and Hough transform plot on the right. A point in the TF plot maps to a sinusoidal curve in the HT plot. A line (signal) in the TF plot maps to a point in the HT plot. The rho and theta values of the point in the HT plot can be used to back-map to the TF plot, in order to find the location of the line (signal) (good if time-frequency plot is cluttered with noise and/or cross-term interference and signal is not visible)

In Figure 1, the image space (time-frequency plot) is on the left and the parameter space (two-dimensional Hough transform plot) is on the right. Each point in the image space maps to a sinusoidal curve in the parameter space. The points 1, 2, and 3 in the image space map to the sinusoidal curves 1, 2, and 3 in the parameter space. In the parameter space, the intersection of the sinusoidal curves 1, 2, 3 at the point rho (x), theta (x) corresponds to the line connecting the points 1, 2, and 3 in the image space (same rho (x) and theta(x) values) [ISI96]. The more sinusoidal curves in the parameter space that pass through a particular point, the higher the accumulator value of that point will be and the higher the three-dimensional Hough Transform 'spike' will be [OLM01]. The presence of a peak in the parameter space reveals the presence of high positive values concentrated along a line in the image space – whose parameters are exactly the coordinates of the peak. The peak in the parameter space is located in a position which depends on the chirp rate of the line in the image space [BAR95]. The two-dimensional Hough transform plot is simply a birds-eye view of the three-dimensional plot, therefore a 'point' (or 'bright spot') in two-dimensional Hough transform plot is equivalent to a 'spike' in the three-dimensional Hough transform plot. The Hough transform converts a difficult global detection problem in the image space into a more easily solved local peak detection problem in the parameter space [THU04].

The Hough Transform of a given function $g(x, y)$is defined in equation (15) as:

$$H_g(\rho,\theta) = \iint_{-\infty}^{+\infty} g(x,y)\delta(\rho - x\cos\theta - y\sin\theta)\,dxdy \quad (15)$$

Where δ is the Dirac delta function. With $g(x, y)$ (as noted in the figure above), each point (x, y) in the original image g, is transformed into a sinusoid $\rho = x\cos\theta + y\sin\theta$, where, in the image, ρ is the perpendicular distance from the center of the image to the line at an angle θ from the vertical axis passing through the center of the image. Again, points that lie on the same line in the image will produce sinusoids that all cross at a single point in the Hough plot.

The expression above gives the projection (line integral) of $g(x, y)$ along an arbitrary line in the x-y plane. By definition, the Hough Transform computes the integration of the values of an image over all its lines.

From the signal location (rho and theta values) of the Hough transform plot, it is possible to back-map back to the signal location in the time-frequency representation, using the same exact rho and theta values.

Let's give an example of back-mapping, starting with the Hough Transform plot in Figure 2:

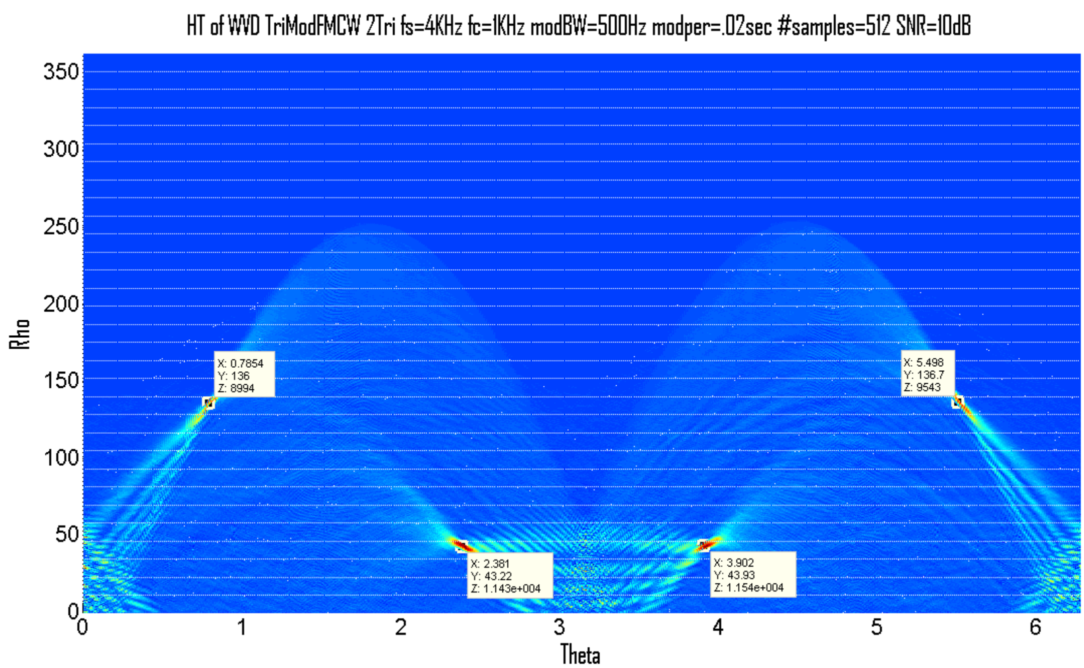

Figure 2: Hough transform of the WVD of a triangular modulated FMCW signal at an SNR of 10dB (512 samples). Each point has a unique theta and rho value which can be used to back-map to the time-frequency (WVD) representation in order to locate the 4 signals, as depicted in Figure 3

4 signals are clearly seen in the Hough transform plot (Figure 2); from left to right they are (theta, rho, intensity):

Signal 1: .7854, 136, 8994
Signal 2: 2.381, 43.22, 11430
Signal 3: 3.902, 43.93, 11540
Signal 4: 5.498, 136.7, 9543

The values of rho and theta allow for back-mapping to the time-frequency distribution in order to determine the location of these 4 signals in the time-frequency distribution.

Theta is in radians, therefore we multiply by 57.3 to obtain degrees.

Rho is the number of samples, therefore we divide by 512 (the number of samples of the Y-Axis of the time-frequency distribution) to obtain rho (length) in terms of percent of the length of the entire Y-Axis of the time-frequency distribution.

Signal 1: 45.0 degrees, 26% of Y-Axis
Signal 2: 136.4 degrees, 8% of Y-Axis
Signal 3: 223.6 degrees, 8% of Y-Axis
Signal 4: 315.0 degrees, 26% of Y-Axis

With these values, we can now back-map from the Hough transform plot (Figure 2) to the time-frequency distribution to find where the 4 signals are located in the time-frequency distribution (Figure 3).

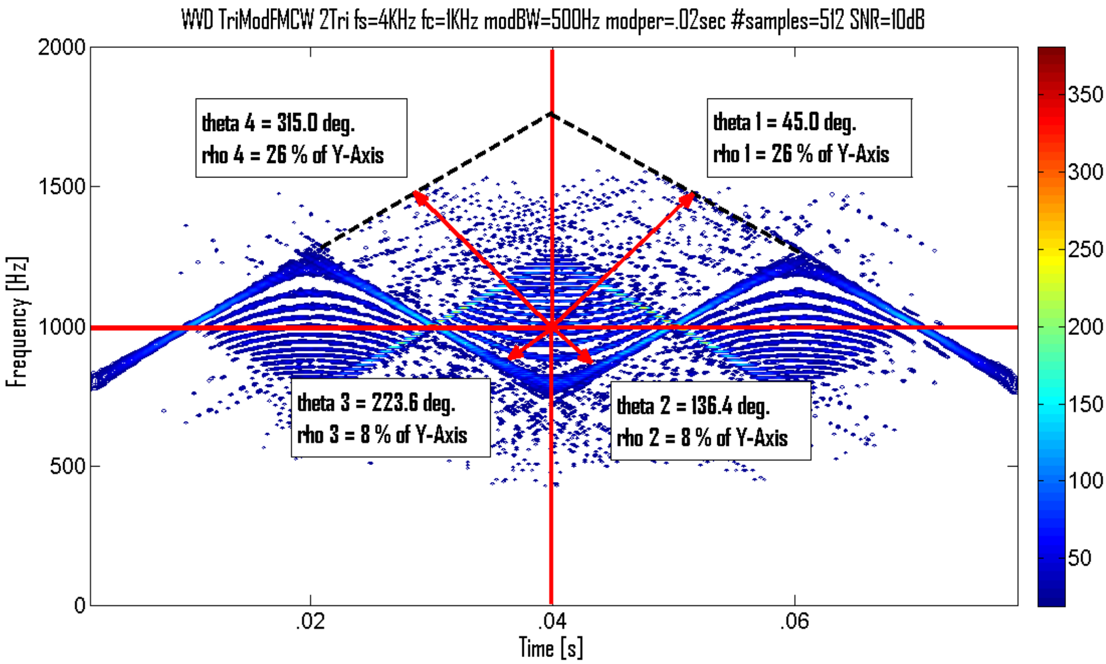

Figure 3: The unique theta and rho values extracted from Figure 2 are used to back-map to the time-frequency representation (WVD of a triangular modulated FMCW signal (SNR=10dB, #samples=512)) in order to locate the 4 chirp signals that make up the 4 legs of the triangular modulated FMCW signal

Figure 3 shows how the unique theta and rho values from the Hough transform plot can be used to back-map to the time-frequency distribution in order to find the location of the signals in the time-frequency distribution. This would be beneficial in the case where the signals in the time-frequency distribution were unable to be seen, due to cross-term interference and/or noise, but the signals were seen in the Hough transform plot. We could then back-map from the Hough transform plot, using the theta and rho values of the signals, to find the location of the signals in the time-frequency representation.

It is important to note that the Hough transform method works well in the presence of multi-component signals, in spite of the cross-terms produced by time-frequency distributions such as the WVD [TOR07]. Since the cross-terms have an amplitude modulation, the integration implicit in the Hough transform reduces them, while the useful contributions, which are always positive, are correctly integrated [BAR92], [BAR95]. Likewise, in the presence of noise, the integration carried out by the Hough transform produces an improvement in the SNR [INC07], [YAS06], [NIK08].

The Hough transform is very similar to the Radon transform. The Hough transform, like the Radon transform is a mapping from image space to parameter space. The Radon transform is usually treated as a reading paradigm (how a data point in the destination space is obtained from the data in the source space). The Hough transform is usually treated as a writing paradigm (how a data point in the source space maps onto data points in the destination space) [GIN04], [ZAI99].

Some additional advantages of the Hough transform are its ability to discard features belonging to other objects and its robustness against incomplete data [CAR06], [BEN05].

The Hough transform finds many uses today, from signal processing (such as low SNR signal extraction and chirp rate determination) to image processing (such as locating iris features in frontal face images [TOE02]).

The ability of the Hough Transform to perform well in low SNR environments, as well as in heavy cross-term environments makes it an ideal signal analysis tool to offset the classical time-frequency analysis deficiencies of cross-term interference and mediocre performance in low SNR environments. This makes for better readability, leading to more accurate parameter extractions for the intercept receiver signal analyst.

The joint sequential use of the RSPWVD and the Hough Transform (HT) will be used in this paper.

II. Methodology

The methodologies detailed in this section describe the processes involved in obtaining and comparing metrics between the joint sequential use of the Reassigned Smoothed Pseudo Wigner-Ville Distribution and the Hough Transform vs. the Reassigned Smoothed Pseudo Wigner-Ville Distribution signal processing techniques for the detection and characterization of low probability of intercept triangular modulated FMCW radar signals.

The tools used for this testing were: MATLAB (version 8.3), Signal Processing Toolbox (version 6.21), and Time-Frequency Toolbox (version 1.0) (http://tftb.nongnu.org/).

All testing was accomplished on a desktop computer (Dell Precision T1700; Processor -Intel Xeon CPU E3-1226 v3 3.30GHz; Installed RAM - 32.0GB; System type - 64-bit operating system, x64-based processor).

Testing was performed for the triangular modulated FMCW waveform, whose parameters were chosen for academic validation of signal processing techniques. Due to computer processing resources they were not meant to represent real-world values. The number of samples was chosen to be 512, which seemed to be optimum size for the desktop computer. Testing was performed at three different SNR levels: 10dB, 0dB, and the lowest SNR at which the signal could be detected. The noise added was white Gaussian noise, which best reflects the thermal noise present in the IF section of an intercept receiver [PAC09]. Kaiser windowing was used, where windowing was applicable. 100 runs were performed for each test, for statistical purposes. The plots included in this paper were done at a threshold of 5% of the maximum intensity and were linear scale (not dB) of analytic (complex) signals; the color bar represented intensity. The signal processing techniques used for each task were the joint sequential use of the Reassigned Smoothed Pseudo Wigner-Ville Distribution and the Hough Transform vs. the Reassigned Smoothed Pseudo Wigner-Ville Distribution.

The triangular modulated FMCW signal (most prevalent LPI radar waveform [LIA09]) used had the following parameters: sampling frequency=4KHz; carrier frequency=1KHz; modulation bandwidth=500Hz; modulation period=.02sec.

After each individual run for each individual test, metrics were extracted from the time-frequency representation. The metrics that were extracted were as follows:

1) *Percent Detection:* Percent of time signal was detected - signal was declared a detection if any portion of each of the signal components (4 chirp components for triangular modulated FMCW) exceeded a set threshold (a certain percentage of the maximum intensity of the time-frequency representation).

Threshold percentages were determined based on visual detections of low SNR signals (lowest SNR at which the signal could be visually detected in the time-frequency representation) (see Figure 4).

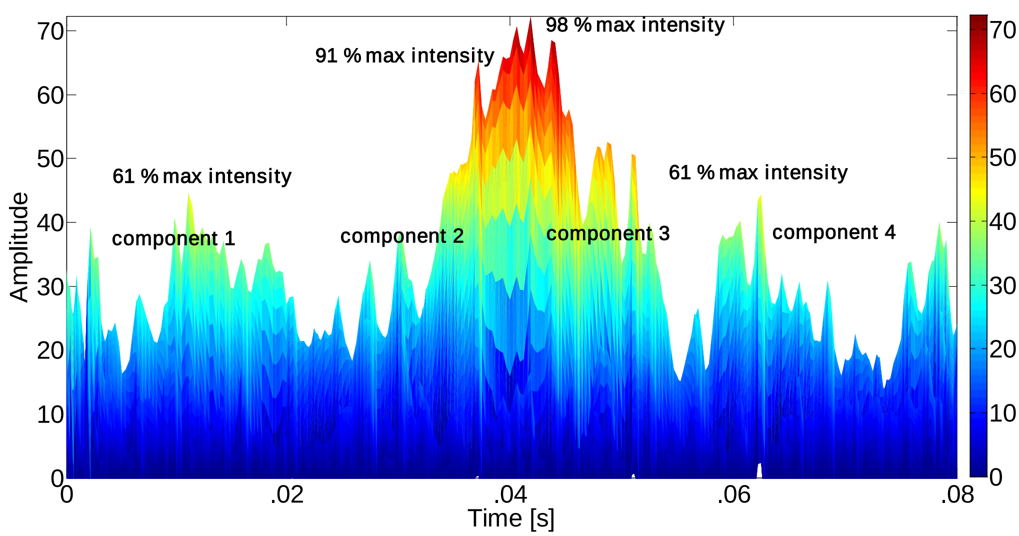

Figure 4: Threshold percentage determination. This plot is a time vs. amplitude (x-z view) of a signal processing technique of a triangular modulated FMCW signal (512 samples, with SNR=-3dB). For visually detected low SNR plots (like this one), the percent of max intensity for the peak z-value of each of the signal components (the 2 legs for each of the 2 triangles of the triangular modulated FMCW) was noted (here 61%, 91%, 98%, 61%), and the lowest of these 4 values was recorded (61%). Ten test runs were performed for this waveform for each of the signal processing techniques that were used. The average of these recorded low values was determined and then assigned as the threshold for that particular signal processing technique

Based on the above methodology, thresholds were assigned as follows for the signal processing techniques used for this paper: RSPWVD + HT (60%); RSPWVD (60%).

For percent detection determination, these threshold values were included for each of the signal processing technique algorithms so that the thresholds could be applied automatically during the plotting process. From the time-frequency representation threshold plot, the signal was declared a detection if any portion of each of the signal components was visible (see Figure 5).

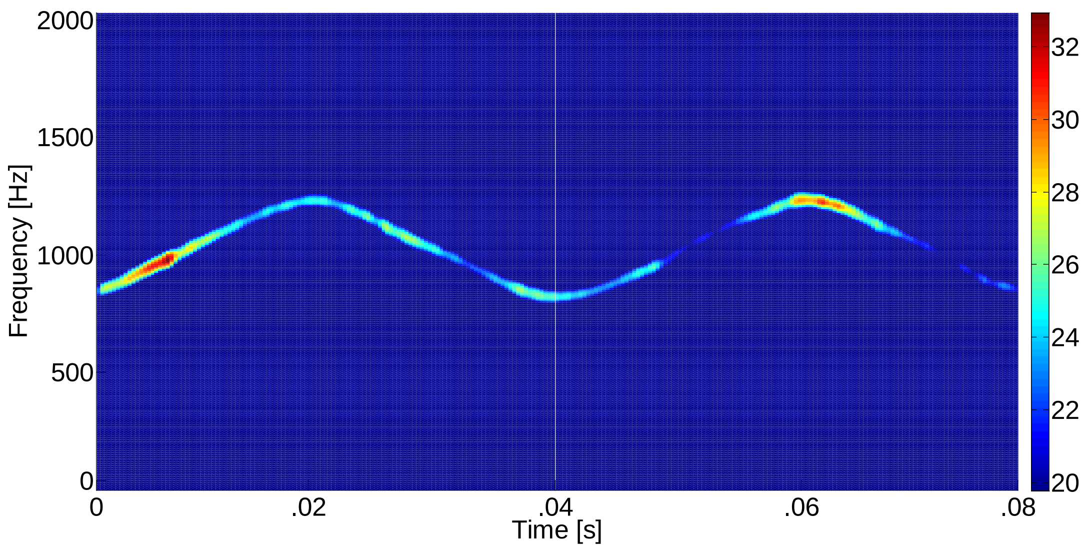

Figure 5: Percent detection (time-frequency). This plot is a time vs. frequency (x-y view) of a signal processing technique of a triangular modulated FMCW signal (512 samples, with SNR=10dB) with threshold value automatically set to 60%. From this threshold plot, the signal was declared a (visual) detection because at least a portion of each of the 4 signal components (the 2 legs for each of the 2 triangles of the triangular modulated FMCW) was visible

2) *Modulation Bandwidth (Note: Modulation bandwidth was used to calculate the Chirp Rate):* Distance from highest frequency value of signal (at a threshold of 20% maximum intensity) to lowest frequency value of signal (at same threshold) in Y-direction (frequency).

The threshold percentage was determined based on manual measurement of the modulation bandwidth of the signal in the time-frequency representation. This was accomplished for ten test runs for each of the signal processing techniques that were used, for the triangular modulated FMCW waveform. During each manual measurement, the max intensity of the high and low measuring points was recorded. The average of the max intensity values for these test runs was 20%. This was adopted as the threshold value and is representative of what is obtained when performing manual measurements. This 20% threshold was also adapted for determining the modulation period and the time-frequency localization (both are described below).

For modulation bandwidth determination, the 20% threshold value was included for each the signal processing technique algorithms so that the threshold could be applied automatically during the plotting process. From the threshold plot, the modulation bandwidth was manually measured (see Figure 6).

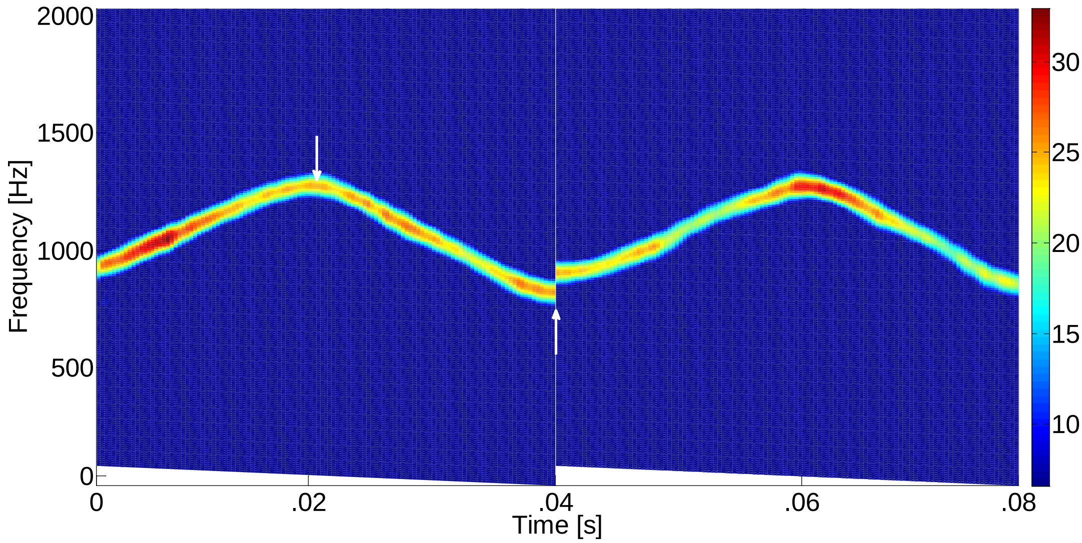

Figure 6: Modulation bandwidth determination. This plot is a time vs. frequency (x-y view) of a signal processing technique of a triangular modulated FMCW signal (512 samples, SNR=10dB) with threshold value automatically set to 20%. From this threshold plot, the modulation bandwidth was measured manually from the highest frequency value of the signal (top white arrow) to the lowest frequency value of the signal (bottom white arrow) in the y-direction (frequency)

3) *Modulation Period (Note: Modulation period was used to calculate the Chirp Rate):* Distance from highest frequency value of signal (at a threshold of 20% maximum intensity) to lowest frequency value of signal (at same threshold) in X-direction (time).

For modulation period determination, the 20% threshold value was included for each of the signal processing technique algorithms so that the threshold could be applied automatically during the plotting process. From the threshold plot, the modulation period was manually measured (see Figure 7).

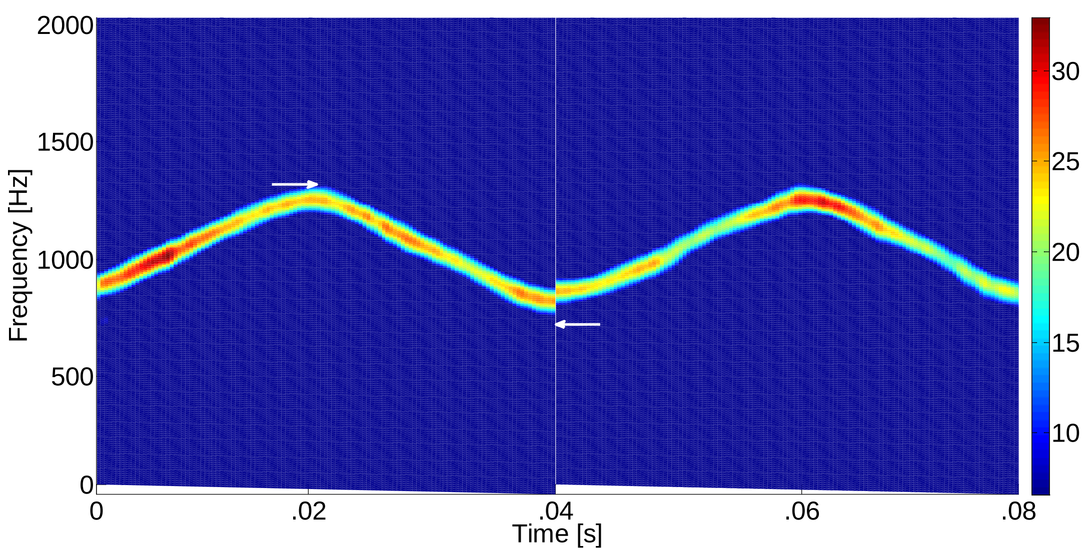

Figure 7: Modulation period determination. This plot is a time vs. frequency (x-y view) of a signal processing technique of a triangular modulated FMCW signal (512 samples, SNR=10dB) with threshold value automatically set to 20%. From this threshold plot, the modulation period was measured manually from the highest frequency value of the signal (top white arrow) to the lowest frequency value of the signal (bottom white arrow) in the x-direction (time)

4) *Chirp Rate:* Equals (modulation bandwidth)/(modulation period)
5) *Lowest Detectable SNR:* The lowest SNR level at which at least a portion of each of the signal components exceeded the set threshold listed in the percent detection section above.

For lowest detectable SNR determination, these threshold values were included for each of the signal processing technique algorithms so that the thresholds could be applied automatically during the plotting process. From the threshold plot, the signal was declared a detection if any portion of each of the signal components was visible. The lowest SNR level for which the signal was declared a detection is the lowest detectable SNR (see Figure 8).

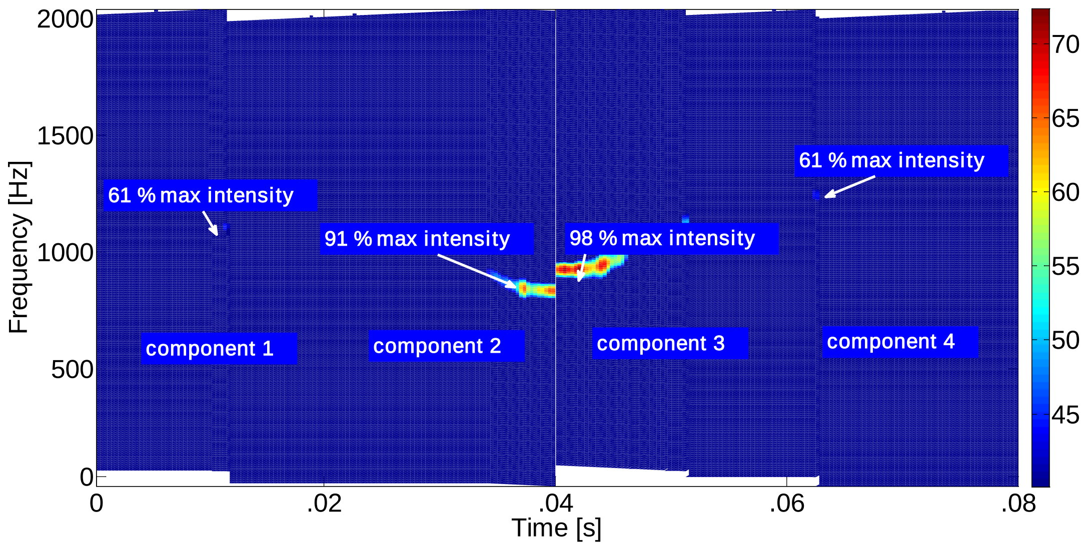

Figure 8: Lowest detectable SNR. This plot is a time vs. frequency (x-y view) of a signal processing technique of a triangular modulated FMCW signal (512 samples, with SNR= -3dB) with threshold value automatically set to 60%. From this threshold plot, the signal was declared a (visual) detection because at least a portion of each of the 4 signal components (the 2 legs for each of the 2 triangles of the triangular modulated FMCW) was visible. Note that the signal portion for the two 61% max intensities are barely visible, because the threshold for this particular signal processing technique is 60%. For this case, any lower SNR than -3dB would have been a non-detect

The data from all 100 runs for each test was used to produce the actual, error, and percent error for each of the metrics listed above.

The metrics for the joint sequential use of the Reassigned Smoothed Pseudo Wigner-Ville Distribution and the Hough Transform, along with the metrics for the Reassigned Smoothed Pseudo Wigner-Ville Distribution were generated. By and large, the joint sequential use of the Reassigned Smoothed Pseudo Wigner-Ville Distribution and the Hough Transform (RSPWVD + HT) outperformed the Reassigned Smoothed Pseudo Wigner-Ville Distribution (RSPWVD), as will be shown in the results section.

III. Results

Table 1 presents the overall test metrics for the two signal processing techniques used for this testing (the joint sequential use of the Reassigned Smoothed Pseudo Wigner-Ville Distribution and the Hough Transform (RSPWVD + HT) versus the Reassigned Smoothed Pseudo Wigner-Ville Distribution (RSPWVD)).

Table 1: Overall test metrics for the two signal processing techniques (RSPWVD + HT vs. RSPWVD) - (chirp rate (average percent error) for SNR = 10dB, 0dB, -3dB; percent detection (average) for SNR = 10dB, 0dB, -3dB; lowest detectable SNR (average)

Parameters	RSPWVD + HT			RSPWVD		
	10dB	0dB	-3dB	10dB	0dB	-3dB
Chirp Rate (avg.% error)	0.41%	0.51%	0.68%	1.58%	2.81%	5.74%
Percent Detection (avg.)	100%	100%	72.8%	100%	92.4%	8.21%
Lowest Detectable SNR (avg.)	[-5.04db]			[-3.02db]		

From Table 1, RSPWVD + HT outperformed RSPWVD in average percent error chirp rate (10dB: 0.41% vs. 1.58%), (0dB: 0.51% vs. 2.81%), and (-3dB: 0.68% vs. 5.74%). RSPWVD + HT outperformed RSPWVD in average percent detection (10dB: 100% vs. 100%), (0dB: 100% vs. 92.4%), and (-3dB: 72.8% vs. 8.21%). RSPWVD + HT outperformed RSPWVD in average lowest detectable SNR (-5.04dB vs. -3.02dB).

Figure 9 shows comparative plots of the RSPWVD (left) vs. the RSPWVD + HT (right) (triangular modulated FMCW signal) at SNRs of 10dB (top row), 0dB (middle row), and lowest detectable SNR (-3dB for RSPWVD and -5dB for RSPWVD + HT) (bottom row).

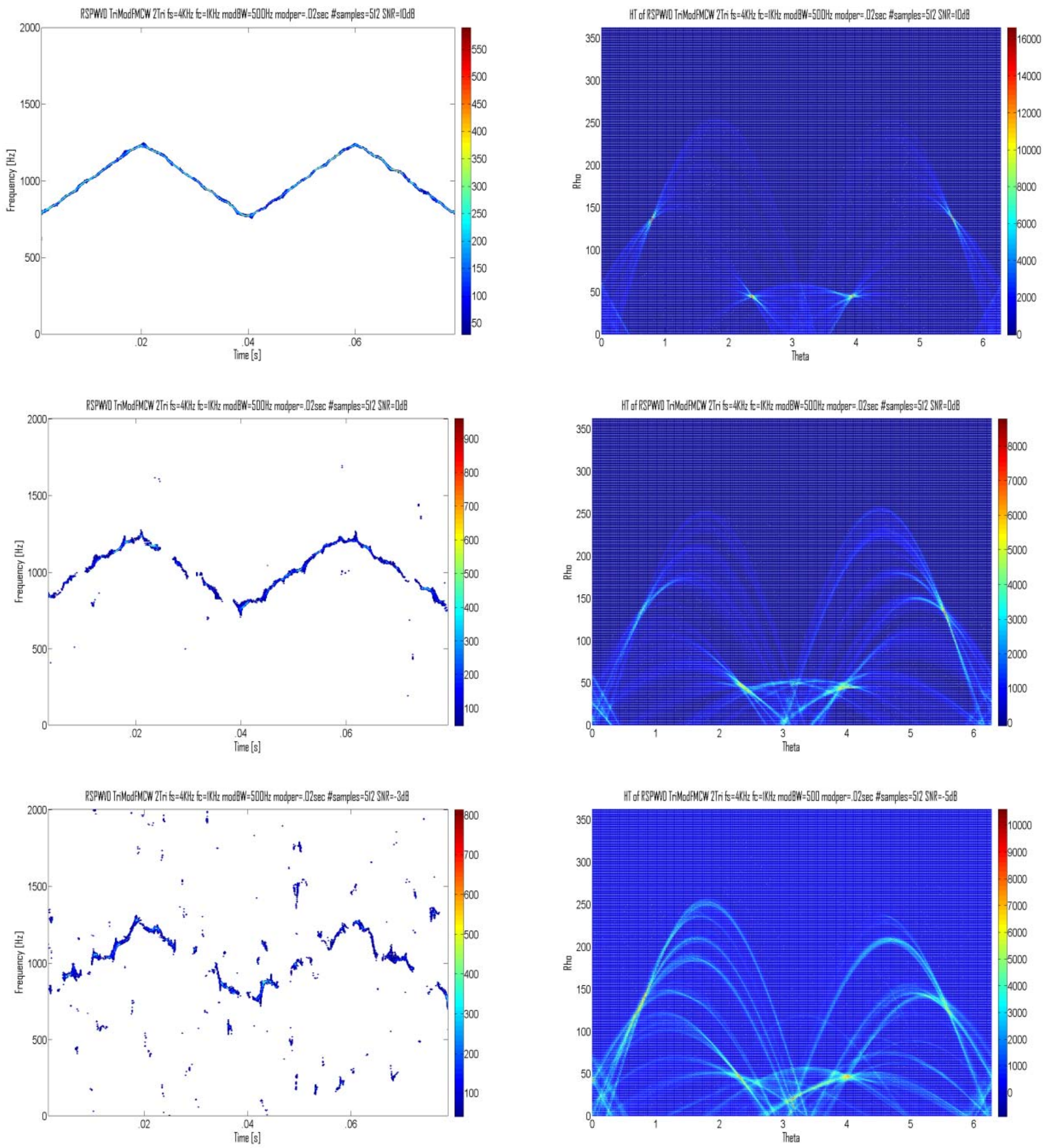

Figure 9: Comparative plots of the triangular modulated FMCW low probability of intercept radar signals (RSPWVD (left-hand side) vs. the RSPWVD + HT (right-hand side)). The SNR for the top row is 10dB, for the middle row is 0dB, and for the bottom row is the lowest detectable SNR (-3dB for RSPWVD; -5 dB for RSPWVD + HT)

IV. Discussion

This section will elaborate on the results from the previous section.

From Table 1, RSPWVD + HT outperformed RSPWVD in average percent error chirp rate (10dB: 0.41% vs. 1.58%), (0dB: 0.51% vs. 2.81%), and (-3dB: 0.68% vs. 5.74%). RSPWVD + HT outperformed RSPWVD in average percent detection (10dB: 100% vs. 100%), (0dB: 100% vs. 92.4%), and (-3dB: 72.8% vs. 8.21%). RSPWVD + HT outperformed RSPWVD in average lowest detectable SNR (-5.04dB vs. -3.02dB).

In previous research it was shown that the reassignment method, with its squeezing and smoothing qualities, reduces cross-term interference of classical time-frequency distributions (i.e. WVD), and produces more localized ('tighter') signals than those of the classical time-frequency distributions, making for improved readability, and consequently the extraction of more accurate metrics than the classical time-frequency distributions [STE21].

In the presence of noise, the integration carried out by the Hough transform produces an improvement in SNR [INC07], [YAS06], [NIK08], and therefore the Hough transform is better able to 'dig' the signal out of noise. This robust performance in low SNR environments translates to improved readability of the Hough Transform plot, and consequently more accurate signal detection and parameter extraction of LPI radar signals.

For the RSPWVD + HT combination, the squeezing quality of the reassignment method, combined with the integration carried out by the Hough transform, makes for 'tighter' signals (equals more accurate theta value extraction and therefore more accurate chirp rate extraction (than for the RSPWVD alone), as per the results in Table 1), and makes for 'higher' signals (equals detecting the signal at lower SNR values (than for the RSPWVD alone), as per the results in Table 1), and better percent detection (than for the RSPWVD alone) due to the signal being that much higher than the noise floor, as per the results in Table 1). Therefore the joint sequential use of the RSPWVD and the HT allows for more accurate signal detection and parameter extraction of LPI radar signals than the RSPWVD alone, making for a more informed, effective, and safer intercept receiver environment, potentially saving valuable equipment, intelligence, and lives.

V. Conclusions

Digital intercept receivers, whose main job is to detect and extract parameters from low probability of intercept radar signals, are currently moving away from Fourier-based analysis and towards classical time-frequency analysis techniques (such as the WVD), and other novel analysis techniques. Though classical time-frequency analysis techniques are an improvement over Fourier-based analysis techniques, classical time-frequency analysis techniques, in particular the WVD, suffer from cross-term interference, which can make the time-frequency representation hard to read, especially if the components are numerous or close to each other, and the more so in the presence of noise. This lack of readability may equate to less accurate signal detection and parameter extraction metrics, potentially placing the intercept receiver signal analyst's platform in harm's way.

In previous research it was shown that the reassignment method, with its squeezing and smoothing qualities, reduces cross-term interference of classical time-frequency distributions (i.e. WVD), and produces more localized ('tighter') signals than those of the classical time-frequency distributions, making for improved readability, and consequently the extraction of more accurate metrics than the classical time-frequency distributions [STE21].

The research in this paper demonstrated that through the joint sequential use of the RSPWVD and the Hough Transform, the squeezing quality of the reassignment method, combined with the integration carried out by the Hough transform, made for 'tighter' signals (equals more accurate theta value extraction and therefore more accurate chirp rate extraction (than for the RSPWVD alone), as per the results in Table 1), and made for 'higher' signals (equals detecting the signal at lower SNR values (than for the RSPWVD alone), as per the results in Table 1), and better percent detection (than for the RSPWVD alone) due to the signal being that much higher than the noise floor, as per the results in Table 1). Therefore the joint sequential use of the RSPWVD and the Hough Transform allows for more accurate signal detection and parameter extraction of LPI radar signals than the RSPWVD alone, making for a more informed, effective, and safer intercept receiver environment, potentially saving valuable equipment, intelligence, and lives.

Future plans include continuing to analyze low probability of intercept radar waveforms (such as the frequency hopping and the triangular modulated FMCW), using additional novel signal processing techniques, and comparing their results with research that has been conducted.

References Références Referencias

1. [ANJ09] Anjaneyulu, L., Murthy, N., Sarma, N., A Novel Method for Recognition of Modulation Code of LPI Radar Signals. International Journal of Recent Trends in Engineering, Vol. 1, No. 3, pp. 176-180, May 2009.
2. [AUG94] Auger, F., Flandrin, P., The Why and How of Time-Frequency Reassignment. IEEE International Symposium on Time-Frequency and Time-Scale Analysis, pp. 197-200, 1994.
3. [AUG95] Auger, F., Flandrin, P., Improving the Readability of Time-Frequency and Time-Scale Representations by the Reassignment Method. IEEE Transactions on Signal Processing, 43(5):1068-1089, 1995.
4. [BAR92] Barbarossa, S., Zanalda, A., A Combined Wigner-Ville and Hough Transform for Cross-Terms Suppression and Optimal Detection and Parameter Estimation. ICASSP '92, Vol. 5, pp. 173-176, 1992.
5. [BAR95] Barbarossa, S., Analysis of Multicomponent LFM Signals by a Combined Wigner-Hough Transform. IEEE Transactions on

Signal Processing, Vol. 43, No. 6, pp. 1511-1515, 1995.
6. [BEN05] Bennett, N., Saito, N., Using Edge Information in Time-Frequency Representations for Chirp Parameter Estimation. Applied Computational Harmonic Analysis, pp. 186-197, 2005.
7. [BOA03] Boashash, B., Time Frequency Signal Analysis and Processing: A Comprehensive Reference. Elsevier, Oxford, England, 2003.
8. [CAR06] Carranza, N., Sroubek, F., Cristobal, G., Motion Estimation by the Pseudo-Wigner Ville Distribution and the Hough Transform. 14th European Signal Processing Conference, Florence, Italy, pp. 1-5, 2006.
9. [CAR94] Carlson, B., Evans, E., Wilson, S., Search Radar Detection and Track with the Hough Transform, Part I: System Concept. IEEE Transactions on Aerospace and Electronic Systems, Vol. 30, No. 1, pp. 102-108, January 1994.
10. [DAH08] Dahyot, R., Bayesian Classification for the Statistical Hough Transform. International Conference on Pattern Recognition, pp. 1-4, December 2008.
11. [DUD72] Duda, R., Hart, P., Use of the Hough Transformation to Detect Lines and Curves in Pictures. Comm. ACM, Vol. 15, No. 1, pp. 11-15, January 1972.
12. [GIN04] Van Ginkel, M., Luengo Hendriks, C., Van Vliet, L., A Short Introduction to the Radon and Hough Transforms and How They Relate to Each Other. Technical Report QI-2004-01, Imaging Science and Technology Department, Delft University of Technology, The Netherlands, 2004.
13. [GUL07] Gulum, T., Autonomous Non-Linear Classifications of LPI Radar Signal Modulations. Thesis, Naval Postgraduate School, Monterey, CA, 2007.
14. [GUL08] Gulum, T., Pace, P., Cristi, R., Extraction of Polyphase Radar Modulation Parameters Using a Wigner-Ville Distribution-Radon Transform. IEEE International Conference on Acoustics, Speech, and Signal Processing, Las Vegas, NV, April 2008.
15. [HAN00] Han, S., Hong, H., Seo, D., Choi, J., Target Position Extraction Based on Instantaneous Frequency Estimation in a Fixed-Reticle Seeker. Opt. Eng., Vol. 39, pp. 2568-2573, September 2000.
16. [HIP00] Hippenstiel, R., Fargues, M., Moraitakis, I., Williams, C., Detection and Parameter Estimation of Chirped Radar Signals. Final Report, Naval Postgraduate School, Monterey, CA, Jan. 10, 2000.
17. [HOU62] Hough, P.V.C., Method and Means for Recognizing Complex Patterns. U.S. Patent 3,069,654, December 18, 1962.
18. [INC07] Incer, I., Kaminsky, E., Performance of Chirp-Slope Keying with Joint Time-Frequency Detectors. Proc. of SPIE Vol. 6577, 6577OH, pp. 1-9, 2007.
19. [ISI96] Auger, F., Flandrin, P., Goncalves, P., Lemoine, O., Time-Frequency Toolbox Users Manual. Centre National de la Recherche Scientifique and Rice University, 1996.
20. [LIA09] Liang, Y., Zhang, L., Xing, M., Bao, Z., High-Speed Ground Moving Target Detection Research Using Triangular Modulation FMCW. Front. Electr. Electron. Eng., China, 4(2), pp. 127-133, 2009.
21. [LIW08] Li, W., Dan, M., Wang, X., Li, D., Wang, G., Fast Estimation Method and Performance Analysis of Frequency Modulation Rate Via RAT. Proceedings of the 2008 IEEE International Conference on Information and Automation, Zhangjiajie, China, pp. 144-147, June 20-23, 2008.
22. [LIX08] Li, X., Bi, G., A New Reassigned Time-Frequency Representation. 16th European Signal Processing Conference, Lausanne, Switzerland, pp. 1-4, August 25-29, 2008.
23. [LIY03] Li, Y., Xiao, X., Recursive Filtering Radon-Ambiguity Transform Algorithm for Detecting Multi-LFM Signals. Journal of Electronics (China), Vol. 20, No. 3, pp. 161-166, May 2003.
24. [MIL02] Milne, P., Pace, P., Wigner Distribution Detection and Analysis of FMCW and P-4 Polyphase LPI Waveforms. Proceedings of ICASSP, Orlando, FL, pp. 3944-3947, 2002.
25. [NIK08] Nikolaev, D., Nikolaev, I., Karpenko, S., Nikolayev, P., Hough Transform: Underestimated Tool in the Computer Vision Field. 22nd European Conference on Modeling and Simulation, Nicosia, Cyprus, June 3-6, 2008.
26. [OLM01] Olmo, G., Magli, E., All-Integer Hough Transform: Performance Evaluation. IEEE Proceedings of the 2001 International Conference on Image Processing, Thessaloniki, Greece, Vol. 13, pp. 338-341, October 7-10, 2001.
27. [OZD03] Ozdemir, A., Time-Frequency Component Analyzer. Dissertation, Bilkent University, Ankara, Turkey, Sept. 2003.
28. [PAC09] Pace, P., Detecting and Classifying Low Probability of Intercept Radar. Artech House, Norwood, MA, 2009.
29. [PAP95] Papandreou, A., Boudreaux-Bartels, G.F., Kay, S., Detection and Estimation of Generalized Chirps Using Time-Frequency Representations. 1994 Conference Record of the Twenty-Eighth Asilomar Conference on Signals, Systems and Computers, pp. 50-54, 1994.
30. [QIA02] Qian, S., Introduction To Time-Frequency and Wavelet Transforms. Prentice Hall, Upper River, NJ, 2002.
31. [RAN01] Rangayyan, R., Krishnan, S., Feature Identification in the Time-Frequency Plane by Using the Hough-Radon Transform. Pattern Recognition, Vol. 34, pp. 1147-1158, 2001.
32. [SHA07] Sharif, R., Abeysekera, S., Efficient Wideband Sonar Parameter Estimation Using a

Single Slice of Radon-Ambiguity Transform. IEEE Transactions on Aerospace and Electronic Systems, Vol. 43, Issue 2, pp. 673-688, April 2007.
33. [STE21] Stevens, D., A Novel Approach for the Characterization of Triangular Modulated Frequency Modulated Continuous Wave Low Probability of Intercept Radar Signals via Application of the Wigner-Ville Distribution and the Reassigned Smoothed Pseudo Wigner-Ville Distribution. Global Journal of Researches in Engineering: F, Electrical and Electronic Engineering, Vol. 21, Issue 2, Ver. 1.0, pp. 19-28, May 2021.
34. [STE96] Stephens, J., Advances in Signal Processing Technology for Electronic Warfare. IEEE AES Systems Magazine, pp. 31-38, November 1996.
35. [THU04] Thuc, N., Duc, D., The Hough Transform – A Radon-Like Transform. 2004 International Conference on Electronic Information, 2004.
36. [TOE02] Toennies, K., Behrens, F., Aurnhammer, M., Feasibility of Hough Transform based Iris Localisation for Real-Time Application. ICPR02, pp. II: 1053-1056, 2002.
37. [TOR07] Toronto, N., Morse, B., Ventura, D., Seppi, K., The Hough Transform's Implicit Bayesian Foundation. IEEE International Conference on Image Processing, Vol. 4, pp. IV-377 – IV-380, October 2007.
38. [WAJ08] Wang, Y., Jiang, Y., Detection and Parameter Estimation of Multicomponent LFM Signal Based on the Cubic Phase Function. EURASIP Journal on Advances in Signal Processing, Vol. 2008, Article ID 743985, pp. 1-7, 2008.
39. [WAN10] Wang, P., Li, H., Djurovic, I., Himed, B., Integrated Cubic Phase Function for Linear FM Signal Analysis. IEEE Transactions on Aerospace and Electronic Systems, to appear, 2010.
40. [WEI03] Wei, G., Wu, S., Mao, E., Analysis of Multicomponent LFM Signals Using Time-Frequency and The Gray-Scale Inverse Hough Transform. IEEE Workshop on Statistical Signal Processing, pp. 190-193, September 28 – October 1, 2003.
41. [WIL06] Wiley, R., ELINT: The Interception and Analysis of Radar Signals. Artech House, Norwood, MA, 2006.
42. [WON09] Wong, K., Davidson, T., Abelkader, S., Detection of Low Probability of Intercept Radar Signals. Defence R&D Canada – Ottawa Contract Report 2009-142, September 2009.
43. [XIA99] Xia, X., Chen, V., A Quantitative SNR Analysis for the Pseudo Wigner-Ville Distribution. IEEE Transactions on Signal Processing, Vol. 47, No. 10, pp. 2891-2894, October, 1999.
44. [XUL93] Xu, L., Oja, E., Randomized Hough Transform (RHT): Basic Mechanisms, Algorithms, and Computational Complexities. CVGIP: Image Understanding, Vol. 57, No. 2, pp. 131-154, March 1993.
45. [YAS06] Yasotharan, A., Thayaparan, T., Optimum Time-Frequency Distribution for Detecting a Discrete-Time Chirp Signal in Noise. IEE Proc.-Vis. Image Signal Process., Vol. 153, No. 2, pp. 132-140, April 2006.
46. [ZAI99] Zaino, J., Bassett, R., et al. An FPGA-Based Adaptive Computing Implementation of Chirp Signal Detection. RAAC, pp. 1-21, 1999.